Silicon (2023) 15:3841–3854
https://doi.org/10.1007/s12633-022-02226-0

ORIGINAL PAPER

Improving the Corrosion Resistance of Magnesium Alloy by Magnesium Phosphate/Glass Composite Coatings Using Sol–Gel Method

Mohammad M. Farag[1] · Hanaa Y. Ahmed[2] · Zainab M. Al-Rashidy[3]

Received: 14 September 2022 / Accepted: 11 November 2022 / Published online: 23 November 2022

Abstract
Coating of Mg alloys with Mg-phosphate is usually performed by complex and costly methods. This work was mainly aimed at using Mg-phosphate ceramic for Mg metal implants by simple and cost-effective spin coating combined with a sol–gel approach. Where, Mg-phosphate ceramic particles were dispersed with different percentages (0, 10, and 30 wt. %) in the glass sol (85 SiO_2 – 10 CaO – 5 P_2O_5 system) as a coating solution. The coated substrates were characterized by TGA, XRD, FTIR, contact angle, and SEM/EDX analyses, and the in vitro bioactivity test was performed in revised simulated body fluid (rSBF). The results showed the coating thickness was 8.8 ± 0.8, 5.4 ± 0.6, and 5 ± 0.7 µm for MP0, MP10, and MP30, respectively. Moreover, the coatings increased the hydrophilicity of the metal surface. All coatings enhanced the formation of an apatite-bone like layer on the Mg metal surface, and they were viable with oral epithelial cells at a concentration ≤ 125 µg/ml. Moreover, MP0 and MP10 coatings significantly enhanced the corrosion resistance of the metal, while; MP30 coating did not show a significant effect on it. Thus, the percentage of Mg-phosphate in the coating was valuable for corrosion resistance when it was ≤ 10 wt. %. As a result, the composite coatings showed promising coatings for Mg metal substrate to enhance its corrosion resistance at low percentages of Mg-phosphate ceramic.

Keywords Mg alloy · Mg-phosphate · Bioactive glass · Spin coating · Sol–gel

1 Introduction

Magnesium alloys are considered one of the most interesting in orthopedics because of their high mechanical properties, low density, bioactivity, and biodegradability. Where there is no need to remove them by the second surgery after the healing of the surgery part because they already degrade inside the body gradually during meanwhile bone healing process [1–3]. Moreover, Mg alloys possess mechanical properties rather similar to the elastic moduli and compressive strength of human cortical bone [4, 5]. However, magnesium alloys have rapid and uncontrollable corrosion in the body. That is because of their acute reaction with chloride ions present in the body fluid [6]. As a result, hydrogen gas evolves during the corrosion process, which causes bubbles at the metal and tissue interface, which results in taking apart the metal implant and losing its function [7]. As well, hydroxyl ions release in the physiological fluids and increase the pH around the metal implant which may be leading to injury to surrounding tissues. The ideal solution to slow down the corrosion of magnesium alloys in the body is transforming their surfaces from highly reacted surfaces to relatively passive ones. This can be performed by alloying [8, 9], energetic radiation surface modification [10, 11], and surface coating [12, 13]. Surface coating is the most preferably used strategy to decrease the corrosion rate of magnesium alloys. Various techniques including plasma spraying, enameling, slurry dipping, electrophoretic deposition, biomimetic process, sputter coating, and sol–gel

✉ Mohammad M. Farag
mmfaragnrc@gmail.com

[1] Glass Research Department, National Research Centre, 33 El Bohouth Str., Dokki 12622, Giza, Egypt

[2] The Regional Center of Mycology and Biotechnology, Al-Azhar University, Cairo, Egypt

[3] Department of Refractoriness, Ceramics and Building Materials, National Research Centre, Dokki 12622, Giza, Egypt

have been utilized for the surface coating of metallic implants [14–17]. The sol–gel method possesses a special interest in metal coating application, that is because of its low coating temperature, coating of complex shapes, high homogeneity, and less contamination [18].

Bioactive coating materials are favored for the coating of magnesium alloy implants. These coatings can induce biological bonding at the metal and tissue interface. Examples of bioactive materials are hydroxyapatite, bioactive glasses, α- and β-tricalcium phosphates, and magnesium phosphate. Bioactive glasses are the most interesting bioceramic materials for bone defects and soft tissue treatments during the last decades. That is because of their unique ability to convert to hydroxyapatite (HA) in vivo, and their ability to bond with the bone and soft tissues [19–21]. The melt-derived bioactive glass was firstly discovered by Hench in 1971 [19], which showed its ability to bond with the bone and certain types of connective tissue through the attachment of collagen to the glass surface. In 1991, the incorporation of sol–gel chemistry gave rise to a new generation of bioactive glasses [22]. It gave advantages and technological significance to bioactive coating materials as well. And so, the sol–gel process is a widely used method for bioactive glass composite metal implant coating [23]. Therefore, there have been numerous studies that applied bioactive glass for Mg alloy coating via a sol–gel process. Omar, et al. studied a change of precursors in the synthesis of sol–gel 58S glass (60 SiO_2—36 CaO—4 P_2O_5 mol %) as coatings for AZ31 and AZ91 magnesium alloys using dip coating. They used tetramethyl orthosilicate and tetramethyl orthosilicate/methyltriethoxysilane as different precursors for silica. They concluded that the glass synthesized by second combined alkoxides of silica decreased the initial degradation rate in the simulated body fluid [21]. Dou, et al. used sol–gel derived 45S5 bioactive glass–ceramic coatings AZ31 magnesium alloy by dip coating technique. The coating thickness ranged from 0.48 to 1.00 µm, and such coating significantly decreased the weight loss of the metal substrate [22, 23]. Huang, et al. applied mesoporous 58S bioactive glass coatings for AZ31 magnesium alloy using the sol–gel dip coating approach. Because of its high surface area and reactivity, mesoporous bioactive glass enhanced the formation of the apatite layer after immersion in the biological fluid, as well as, increased the corrosion resistance of the metal substrate [24]. Yang, et al. prepared composite coatings based on 45S5 bioactive glass nanoparticles and polycaprolactone polymer for pure magnesium metal using the spin coating method [25]. Akram, et al. coated Mg-Si-Sr alloy with chitosan/gelatin/bioactive glass composite coatings by electrophoretic deposition using alternating current fields and studied different parameters, such as the coating suspension, frequency, voltage amplitude, and time. Their results concluded that the established coatings effectively reduced the corrosion to 0.08 mm/year for coated one compared to 0.69 mm/year of uncoated metal [26].

Application of bioactive composites for Mg alloy coating application is more desired because different physical and chemical properties can be tailored. In our previous study, we introduced Mg-phosphate in the bioactive glass and got composites with controllable biodegradation. Where we prepared composites based on nanobioactive glass and Mg-phosphate, and the results showed that the addition of Mg-phosphate improved the cell viability, and controlled the degradation of the scaffolds [24]. Recently, Mg-phosphate ceramics reported as versatile bioceramic materials for bone regeneration due to their good biocompatibility with bone-forming cells [25–28]. Moreover, the cements derived from Mg-phosphates are is characterized by high mechanical strength comparable to other bone substitutes [29], and so, they used successfully in dentistry and orthopedics [30]. Hence, Mg-phosphate has been used for coating magnesium alloys, For example, not limited to, Van Phuong, et al. developed Mg-phosphate and Zn-phosphate coatings for AZ31 magnesium alloy by immersing the alloy in Mg-phosphate and Zn-phosphate solutions, and compared between them from the view of corrosion behavior [31]. In a similar study, Zai, et al. performed conversion coatings for AZ31 Mg alloy by Mg-phosphate, Zn-phosphate, and Ca-phosphate and compared the corrosion resistance and biocompatibility of such alloy [32]. Bai, et al. established Mg-phosphate coating on Mg-Zn-Ca alloy by micro-arc oxidation of this alloy, followed by dip coating in a chitosan solution [33]. Anawati, et al. synthesized magnesium phosphate coating on AZ31 magnesium alloy using plasma electrolytic oxidation at different current densities [34]. However, most of the methods applied for coating Mg alloys with Mg-phosphate are performed by phosphate chemical conversion process, arc oxidation, and plasma oxidation. Which are likely expensive and time consumed in the most context. So, introducing Mg-phosphate ceramic in the coating of Mg alloy by a simple and cost-effective method is a critical issue.

In this work, we presented new bioactive glass/Mg-phosphate ceramic composite coatings for Mg alloys using the sol–gel method combined with the simple spin coating. According to our knowledge, the published works that address this type of composite coatings are very scarce. The main idea is to take advantage of the best properties of each component that forms the composite coatings. In particular, such composite coatings are expected to combine the bioactive properties of bioglass and the good bioresorbability and biocompatibility of Mg-phosphate ceramics.

2 Materials and Methods

2.1 Preparation of Mg Phosphate (MP) Ceramic

The suggested Mg-phosphate in this work was based on $Mg_3(PO_4)_2$ composition, and it was synthesized by the reaction of $MgCl_2.6H_2O$ (Sigma, Germany) and H_3PO_4 (Sigma, Germany), with Mg/P molar ratio of 1.5. H_3PO_4 solution was added to $MgCl_2.6H_2O$ solution dropwise and the solution was stirred for 3 h. Then, the pH of the solution was adjusted to 9 by using 3 M NaOH to precipitate the Mg-phosphate gel. The gel was left for 24 h for aging and it was washed several times with distilled water and dried at 60 °C for 2 days. The final dry gel was used as-received with glass for the coating process.

2.2 BG/MP Sol–Gel Coatings

The glass composition based on 85 SiO_2—10 CaO—5 P_2O_5 was prepared using the sol–gel method. The following chemicals with analytical grades were used as received to synthesize glasses by a quick alkali-mediated sol–gel method. TEOS (tetraethyl orthosilicate Sigma, Germany), $Ca(NO_3)_2{\cdot}4H_2O$ (99%, Alfa aser, USA) and TEP (triyethyl phosphate (99%, Alfa aser, USA)), ethanol (EtOH), Sigma, Germany, 1 M hydrochloric acid (HCl), Sigma, Germany and ethylene glycol, EG (was added to enhance viscosity and silica condensation), Sigma, Germany. In a typical synthesis of BG sol, TEOS was added to a mixture of 1 M HCl and ethanol solution. TEOS: EtOH: H_2O: EG was 1: 1: 1: 0.65 molar ratio. After complete hydrolysis of TEOS, TEP and $Ca(NO_3)_2{\cdot}4H_2O$ were added to the solution, respectively, with 30 min time interval, and the solution was left to stir for 3 h. and then, different weight percentages of MP powder were added with different weight ratios (0, 10 and 30 wt. %), and samples accordingly encoded MP0, MP10, and MP30, respectively, and the blank Mg metal was used for comparison. The powder was dispersed well in the glass sol by stirring for 1 h and sonicated for 30 min. and used for coating Mg substrates thereafter.

The Mg metal substrate (99.9% metals basis) was cut into small pieces of 1×1 cm and polished with SiC paper in series sizes 240, 600, and 1200 grits. And then, they were washed with ethanol several times and cleaned by ultrasonic in ethanol solution to remove any attached impurities.

The coating process was carried out by the spin coating technique. Where 100 µm of glass sol or glass sol/MP was distributed on the whole metal substrate surface, the spin coater was adjusted to a speed of 3000 rpm, and the spin time was 60 s. the final coated substrate was dried at room temperature in a covered Petri dish for 1 d.

2.3 Characterization of BG/MP Composite Coatings

The obtained composite coatings were characterized by thermogravimetric analysis (TGA) using TGA Q500 device (USA) in the temperature range 25—1000 °C at a rate of 10 °C.min^{-1} to verify the thermal decomposition behavior of the coatings. the crystalline phases formed on the surface of coated Mg metal substrates were determined by X-ray diffraction (XRD) using a Philips PW1390 X-ray diffractometer (U.S.D.) (UK) in the 2θ range 10—90º in 0.02º steps using CuKα radiation (1.5418 Å). The vibration modes of the chemical functional groups were determined for the coated metal by Fourier transform infrared (FTIR) spectroscopy in the of between 4000 and 400 cm^{-1} wavenumber range using JASCO FT/IR-4600, Japan. The microstructure, coating thickness, and elemental analysis of coating surfaces were clarified by scanning electron microscope coupled with X-ray energy dispersive analysis (SEM/EDXA) by Quanta 250 FEG (Field Emission Gun), Spain, where the sample surface was coated with a thin layer of gold prior to the SEM examination. Moreover, the degree of wettability of the coated metal substrates was determined by contact angle measurement according to ASTM D724-99 and ASTM D5946-96 method. Where of 250 µl of distilled water was dropped on the sample surface and took a photo by horizontal plate camera perpendicular to liquid droplet plane using Compact Video Microscope (CVM) (SDL-UK).

2.4 In Vitro Degradation Test

The in vitro biodegradation test was evaluated in the revised simulated body fluid (rSBF) at pH 7.4 prepared according to the published protocol [35]. The coated Mg metal substrates of 10×10 mm dimension were immersed in the polyethylene cups containing rSBF solution. The immersion solution was completely collected and replaced by the same volume of fresh rSBF at predetermined times (1, 3, 7, 14, 21, and 28 days). Ca and Mg ions concentrations released from the samples into the solutions were measured by inductively coupled plasma optical emission spectroscopy using Optima 8000, Perkin Elmer. In addition, the variation in pH of the incubating liquid was determined as a function of time. Furthermore, the degradation rate per day of the samples was measured and calculated. Finally, the alteration of the coated substrate surfaces after immersion in rSBF was explored by scanning electron microscope coupled with energy dispersive X-ray analysis by Quanta 250 FEG (Field Emission Gun), following the previously mentioned method.

3 Evaluation of the Corrosion Resistance

3.1 Electrochemical Measurement

The electrochemical tests were performed in Hank's solution to compare the electrochemical corrosion properties between bioglass coating and bioglass with a magnesium phosphate coating. Before each test, the surface dimensions of the samples in contact with the electrolyte were measured. Electrochemical measurements were conducted using a potentiostat (Gamry 3000) in a traditional three-electrode cell configuration, platinum was used as the counter electrode, saturated calomel electrode (SCE) was used as a reference electrode and the specimen was used as a working electrode. The specimens of "Mg metal" and coated samples were firstly immersed in Hank's solution for 30 min to acquire a stable open circuit potential (OCP). Then, the potentiodynamic polarization (PDP) test was conducted at the scan rate of 0.5 $mV \cdot s^{-1}$ so that the corrosion reaction can approach a steady state [36, 37]. The initial polarization of the cathodic potential is from -0.5 V versus OCP. Considering the passivation behavior of the anode, the anodic scanning potential ends at 1 V versus OCP. The corrosion currents were determined using Tafel extrapolating. The standard deviations of the corrosion current densities and corrosion potentials were also determined. The mean value and standard deviations of the results were calculated. The pH value of Hank's solution is 7.4 and doesn't need to be adjusted.

3.2 Cell Viability Test

By using the MTT assay, the viability of oral epithelial cells (OEC) following exposure to coated samples (MP0, MP10, and MP30) and uncoated magnesium metal Mg was assessed. OEC (oral epithelial cell line) was cultivated in RPMI media for 24 h until confluence, then treated with various substances and incubated for another 24 h at 37 °C. The culture supernatant was replaced with fresh media after incubation (24 h). The cells in each well were then treated with MTT solution (5 mg/ml) for 4 h at 37 °C. The MTT solution was withdrawn after 4 h of incubation, and DMSO was then applied to each well. Using a microplate reader (SunRise TECAN, Inc., USA), the absorbance was found at 570 nm (Wilson, 2000). A digital camera and an inverted microscope (CKX41; Olympus, Japan) were used to take pictures of the treated cells.

3.3 Statistical Analysis

The experimental data obtained in this study were expressed as the average ± standard deviation (SD) for $n = 3$ and were analyzed using the standard analysis of the Student's t-test. The level of significance (p-value) was set at < 0.05.

4 Results and Discussion

4.1 Thermal Gravimetric Analysis (TGA)

The TGA curves of MP0, MP10, and MP30 coatings are shown in Fig. 1. It can be seen from the figure that there were two stages of thermal decomposition for all samples; the first stage was under 220 ºC which was assigned to water evaporation and condensation of silanol groups [38]. The second stage ranged from 220 ºC to 580 ºC which was attributed to the combustion of organic components and nitrates. Afterward, there was no more weight loss which indicated the formation of stabilized glass and glass/MP composite coatings.

4.2 Contact Angle

The water contact angle method was utilized to know the wettability of magnesium metal substrate after coating and to determine the uniformity and tightness of the coating layer [39]. Figure 2 shows the contact angle measurements (a) and water drop micrographs (b) of Mg, MP0, MP10, and MP30 samples. It is known that the substrate is hydrophobic if the contact angle (θ) is ≥ 90°. Herein, the water contact angle on bare magnesium substrate (sample Mg) was about

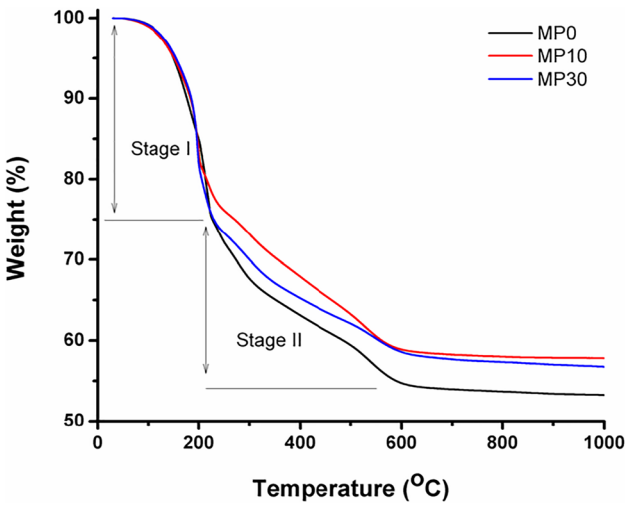

Fig. 1 TGA curves of coated magnesium metal samples; MP0, MP10, and MP30

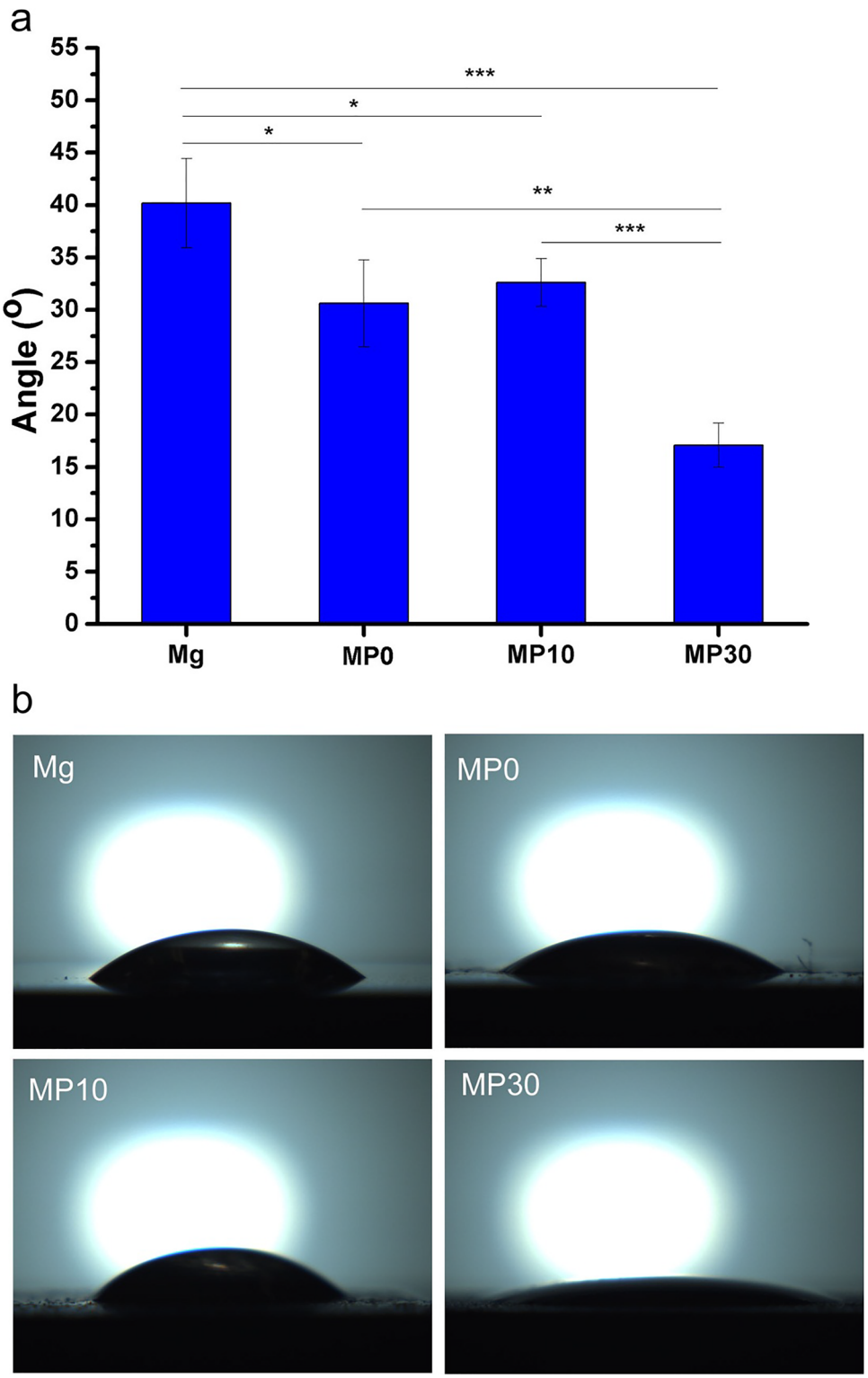

Fig. 2 (**a**) contact angle measurements. (**b**) immediately captured images of water droplet after deposition on Mg metal substrate, MP0, MP10, and MP30 samples. * $p < 0.05$, ** $p < 0.004$ and *** $p < 0.0006$

40°, which indicated its hydrophilicity. Coating of such substrate either by the glass or glass/MP significantly ($p < 0.05$) decreased the contact angles, where, it became 31°, 33°, and 17° for MP0, MP10, and MP30, respectively. This was attributed to the hydrophilicity of silicate glass and Mg phosphate ceramic. Where the silicate groups in the glass frameworks form silanol (Si–OH) groups in an aqueous media. These groups can form hydrogen bonding with the water molecules, and so causing a hydrophilic nature of the coated metal substrate. Moreover, an increase in the wt. % of Mg phosphate ceramic particles significantly decreased the contact angle, this was likely due to the high hydrophilicity

of Mg phosphate ceramic particles and the increase of coating roughness resulting from the inclusion of those particles as shown in Fig. 7. The higher hydrophilicity is desirable for body cell attachment, spreading, and proliferation [40].

4.3 XRD

XRD analysis was performed to detect the formation of new crystalline phases formed on the metal substrate after the coating process. Figure 3a shows XRD diffraction patterns of the coated substrates (MP0, MP10, and MP30) compared to the uncoated magnesium metal (sample Mg). The diffraction patterns of all samples were similar which corresponded to the diffraction pattern of Mg metal (JCPDS Card # 35–0821). The existence of Mg metal peaks in all samples can be assigned to the X-ray penetration through the coatings to the metal substrate. Specifically, the formed coatings were possessed amorphous nature which confirmed by XRD analysis. Where the as-prepared Mg-phosphate particles showed a very weak diffraction pattern (Fig. 3b), these particles were embedded in the amorphous sol–gel derived glass matrix.

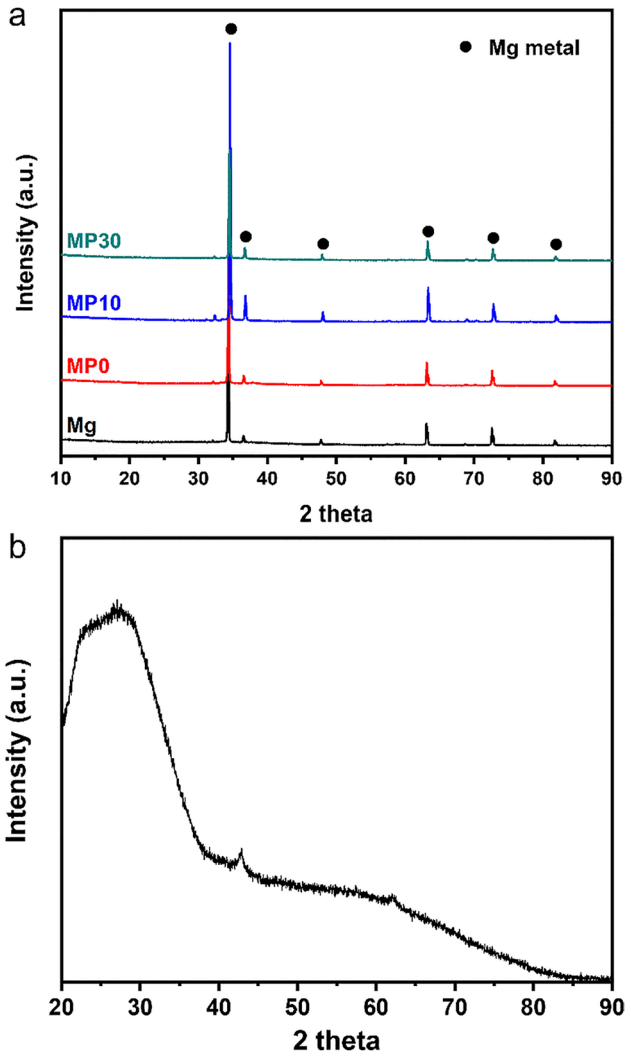

Fig. 3 XRD patterns of (**a**) Mg, MP0, MP10, and MP30 samples, and (**b**) as-prepared Mg-phosphate ceramic

4.4 FTIR

The characteristic groups in different composite coatings were determined by FTIR technique. Figure 4 shows FTIR vibration mode spectra of Mg, MP0, MP10, and MP30 samples. It can be noticed from the figure that the bands centered at 880 cm^{-1} and 1005 cm^{-1} were attributed to the bending vibration mode of O-Si–O and asymmetric stretching of Si–O-Si vibration mode, respectively [41]. The shoulder detected at 1180 cm^{-1} was assigned to the bending vibration mode of Si–O-Si [41]. These bands were stronger for substrate coated with glass only (sample MP0) than that coated with glass and Mg-phosphate (sample; MP10 and MP30). The P-O bending mode was noted at 435 cm^{-1}. Moreover, additional bands at 775 cm^{-1} and 607 cm^{-1} were ascribed to P-O-P bending vibrations. The absorption band at 1418 cm^{-1} was attributed to O–H bending of ethanol and Si–OH.

4.5 Morphology and Elemental Composition of Coatings

Figure 5 shows SEM micrographs and EDX analysis of the magnesium metal substrate (sample Mg), the coated substrates (MP0, MP10, and MP30 samples). It can be noted from the figure that both MP10 and MP30 coatings showed more crack propagation than MP10 coating. The cracks generated on the surface of the substrate coated with glass (sample MP0) were likely due to the shrinkage of the coating layer after glass condensation and evaporation of water and

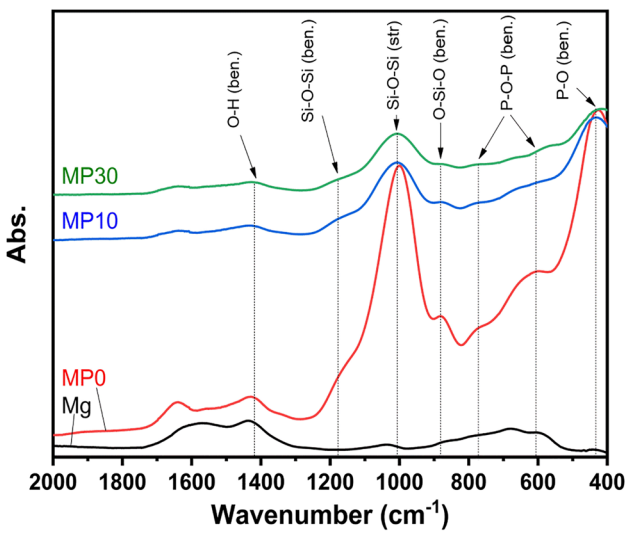

Fig. 4 FTIR spectra of Mg, MP0, MP10 and MP30 samples

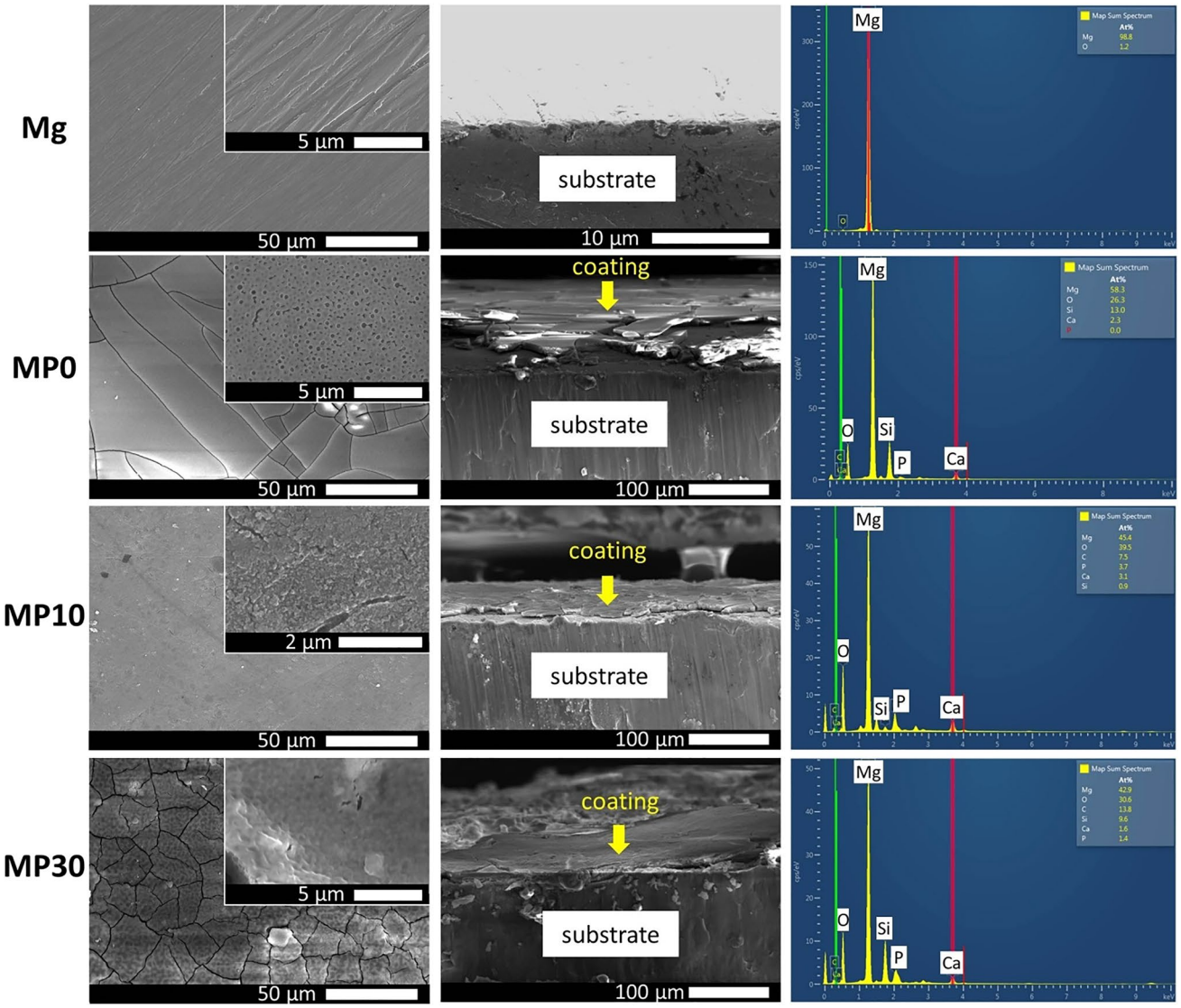

Fig. 5 SEM micrographs of top view with large magnification photo at the upper right corner (left), cross section (middle), and EDX analysis (right) of magnesium metal substrate (sample Mg), and coated substrates (samples; MP0, MP10, and MP30)

ethanol, while, the cracks observed in MP30 coating can be assigned to the creation of fracturing at the ceramic grain-sol interface. In addition, sub-micron pores were detected in the glass coating. Thus, the optimum percentage of Mg phosphate was 10 wt. % which showed crack-free coating. The EDX analysis showed in Fig. 5 and Table 1. The analysis demonstrated that the atomic percentages of different elements were close to the starting percentages of glass and Mg phosphate composites. On the other hand, the EDX mapping of Mg, Si, Ca, and P atoms (data are not shown) showed homogeneous distribution of different elements indicating homogeneous coating and good Mg-phosphate ceramic particle distribution. Furthermore, the coating thickness was measured from SEM photos (photos are not shown) and is stated in Table 1. The coating thickness of glass (sample MP0) was 8.8 ± 0.8 µm which is higher than that of composite coatings; 5.4 ± 0.6 µm and 5 ± 0.7 µm for MP10 and MP30, respectively.

Table 1 Coating thickness (µm) and atomic % of Mg, Si, Ca and P elements analysed by EDX

Sample	Mg	MP0	MP10	MP30
Coating thickness (µm)				
	-	8.8 ± 0.8	5.4 ± 0.6	5 ± 0.7
Atomic %				
Mg	98.8	45.5	85.6	49.8
O	1.2	34.8	7.7	35.5
Si	-	16.4	5.8	11.2
Ca	-	3.2	0.8	1.9
P	-	0.1	0.1	1.6

4.6 In Vitro Bioactivity

An immersion of materials in the SBF (simulated body fluid) to assess an ability to induce the formation of bone-like apatite crystals on their surfaces is still a standard non-cellular in vitro method to investigate the material bioactivity. This newly formed bone-like apatite layer enables the material to make a chemical bond at the material surface and living cell interface. Figure 6 shows SEM micrographs with larger magnification (top and middle) and EDX analysis of Mg, MP0, MP10, and MP30 after immersion in rSBF for 28 d. The new crystals were observed on the surfaces of all samples, these crystals were likely one species of Ca phosphate, which can be confirmed from EDX analysis by increasing the percentage of Ca and P compared to that in samples before SBF immersion (Fig. 5). The atomic Ca/P molar ratios were found at 3.60, 2.56, 0.84, and 1.36 for Mg metal, MP0, MP10, and MP30, respectively. The Ca/P ratio of MP30 was closer to the stoichiometric hydroxyapatite ratio (1.67) than in the other samples. Thus, a modification of the glass coating with Mg-phosphate particles showed a significant effect on the in vitro bioactivity of the final coating. However, the computed Ca/P ratio may be overlapped with the original phosphorus present in the glass and Mg-phosphate ceramic. In addition, soaking of the coated substrates resulted in the appearance of cracks in a micron-scale on their surfaces. This can be explained by the erosion and abrasion of the coatings caused by the soaking fluid which led to a gradual decomposition of those coatings. These cracks caused corrosion beneath the magnesium metal surface.

Moreover, the biodegradation of the coated substrates was investigated by measuring the pH variation, and concentrations of Mg^{2+} and Ca^{2+} ions in the incubated fluid (Fig. 7). The change of pH of rSBF incubated Mg metal, MP0, MP10, and MP30 was investigated at predetermined times. Figure 7a shows the variation of pH of rSBF as a function of time after soaking of samples up to 28 days. It can be noted from the figure that the changes in the pH values of rSBF incubated in all samples were approximately similar. The pH values abruptly increased during the first day of immersion to 8.7, 8.9, 9.0, and 8.7 for Mg, MP0, MP10, and MP30, respectively. This was a result of the release of Mg^{2+} ions from the magnesium metal and form $Mg(OH)_2$ which caused an increase in pH of the solution. A tiny layer of $Mg(OH)_2$ was formed on the uncoated magnesium metal, this layer can attract Ca and P ions from the solution to form hydroxyapatite crystals thereafter. Moreover, the pH of the solutions incubated in the substrates coated with either glass or composites was increased due to a rapid ion exchange between Ca^{2+} (present in glass) and H^+ or H_3O^+ exist in rSBF solution which caused an increase of hydroxyl groups in the solution, and so, rising of the fluid pH. This exchange resulted in the breaking of Si–O-Si glass network bonds and formed silica-rich layer composed mainly of SiOH

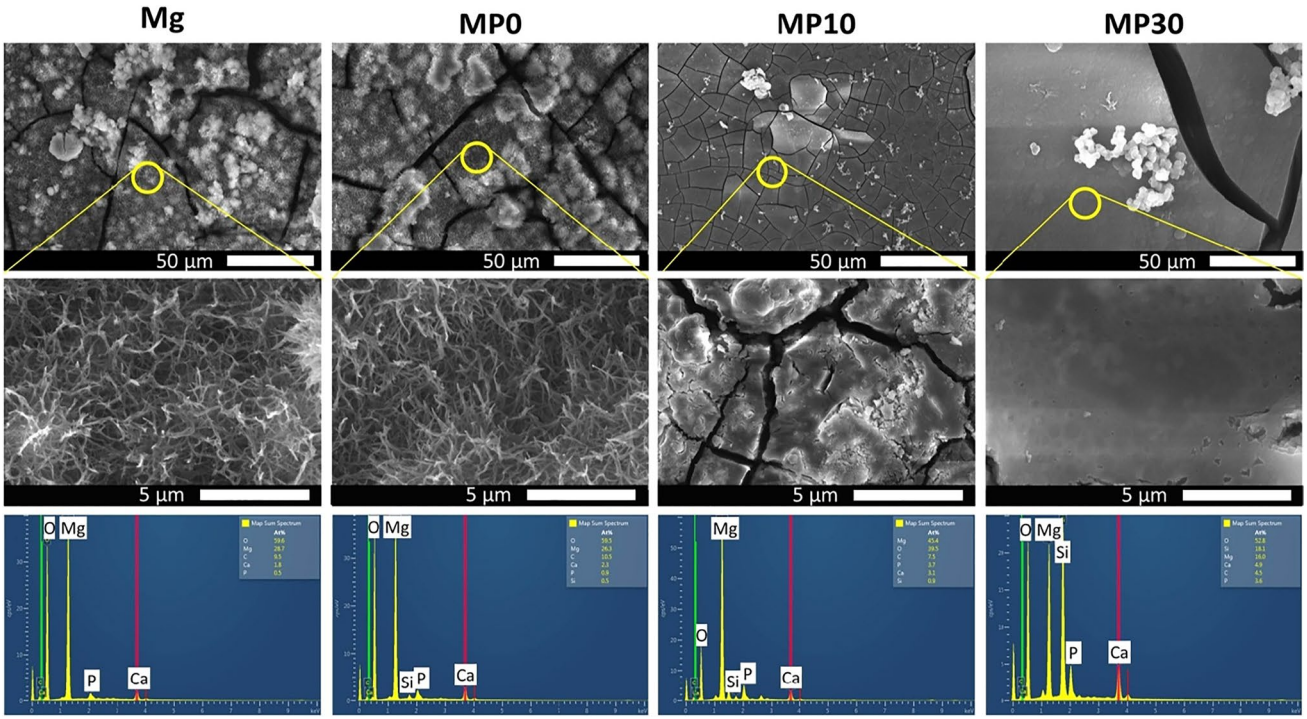

Fig. 6 SEM micrographs with larger magnification (top and middle) and EDX (bottom) analysis Mg, MP0, MP10, and MP30 after immersion in rSBF for 28 d

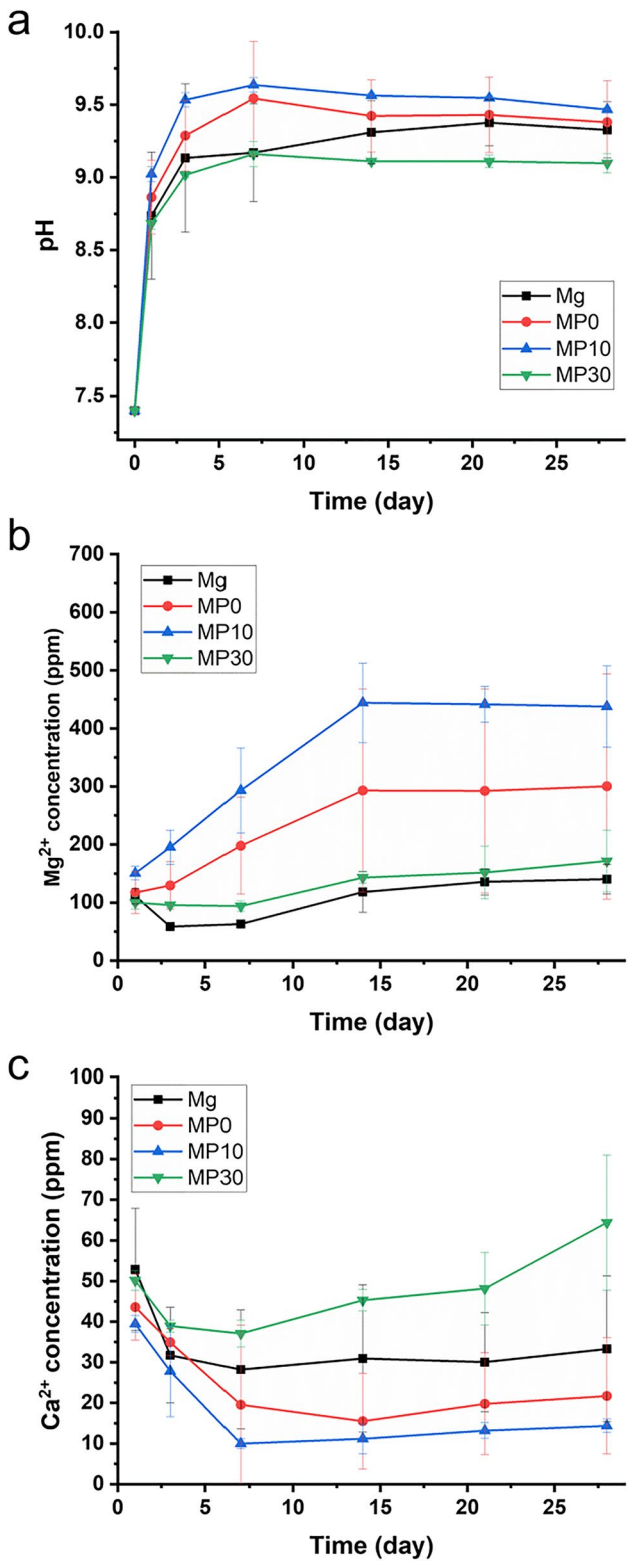

Fig. 7 (**a**) pH, (**b**) Mg^{2+} ion concentration in ppm, and (**c**) Ca^{2+} ion concentration in ppm (**d**) of Mg, MP0, MP10, and MP30 after immersion in rSBF for 28 d

(silanol) groups on the glass surfaces. This newly formed layer possessed the affinity to attract Ca^{2+} and PO_4^{3-} from the surrounding solution and subsequently formed bone-like apatite crystals [42]. After an initial increase in pH values, it became nearly constant between 3 and 28 d, due to the decrease in the formation of hydroxyapatite reaction rate.

The concentrations of Mg^{2+} and Ca^{2+} ions in rSBF were also measured as a sign of degradation rate assessment and hydroxyapatite formation on the coating surfaces (Figs. 7b and c). It can be observed from the figure that Mg^{2+} ions were released in a two-stage behavior. The first stage was a fast release stage which was observed between 1 and 14 d. The second stage was a steady state release stage which was noted between 14 and 28 d. The concentration of Mg^{2+} ions incubated MP10 sample was the highest one, while, the solution incubated Mg metal and MP30 were the lowest concentrations. The concentration of Ca^{2+} ions was reversed to that of Mg^{2+} ion. These can be explained by likely substitution of Mg^{2+} ions by Ca^{2+} ions to form new crystals of Ca-phosphate. Moreover, the concentration of Ca^{2+} ions in the fluid incubated MP30 after 7 d was increased likely due to redissolution of Ca-phosphate layer initially formed on the coated substrate.

Magnesium alloys possess fast and uncontrolled corrosion in the physiological fluid in the body. That is due to the severe reaction with chloride ions that exist in this fluid [6] according to the following reaction:

$$Mg(s) + 2H_2O(aq) \rightarrow Mg(OH)_2(s) + H_2(g)_{\uparrow} \quad (1)$$

Thus, the surface of magnesium alloy is covered ultimately with $Mg(OH)_2$ layer. This layer is greatly reactive with the chloride ions in the body's physiological fluid and quickly converted to soluble $MgCl_2$ according to the following equation [43]:

$$Mg(OH)_2(s) + 2Cl^-(aq) \rightarrow MgCl_2 + 2OH^-(aq) \quad (2)$$

The evolution of hydrogen gas (H_2) gas bubbles, as shown from the above corrosion reactions, at the implant and tissue interface causes disassembling of the metal implant and the loss of its role in bone fixation [7]. Furthermore, the release of hydroxyl ions from the surface of magnesium metal in the physiological solutions increases the alkalinity around the metal implant, and so, affects the pH balances in these solutions which may be leading to poisoning of surrounding tissues. These reactions occur once the Mg metal is soaked in the physiological fluid, like rSBF which explains the abrupt increase in the pH of incubating rSBF. This stage is followed by nearly constant values of pH due to the gradual thickening of the formed $Mg(OH)_2$ layer with time which acted as a corrosion shield layer, and slow down the corrosion reaction, as reported in the previous study [44]. Despit the electrochemical corrosion analyses (as it will be discussed) showed MP30 coating did not increase the corrosion resistance compared to MP0 and MP10 coatings, the concentration of Mg^{2+} ions in the solution incubated MP30 samples was lower than that incubated MP0 and MP10, this

can be attributed to fast reprcipitation of Mg ions as somekind of Mg-phosphate crystals on the coating surface, as it was reported in our previous works [24, 27, 45, 46]. So, the corrosion behavior of Mg alloys goes as initial fast corrosion followed by slow corrosion [47]. Similarly, this explained the nearly constant concentration of magnesium and calcium ions in the later stage of incubation. On the other hand, the measurement of calcium ions in different solutions revealed that the fluid incubated MP10 sample showed a relatively low concentration which can be indicated to consuming of calcium ions in the formation of a new apatite layer, and thus MP10 coating was likely better induced formation of bone-like apatite layer than the other coatings.

4.7 Corrosion Resistance of the Coatings

4.7.1 Electrochemical Corrosion Analysis

Figure 8 shows optical micrographs, the Tafel polarization curves, potential (V), and current density ($A.cm^{-2}$) of coated and uncoated metal substrates in Hank's solution. Also, the corrosion potential (E_{corr}) and corrosion current density (i_{corr}) are listed in Table 2. It can be observed from the optical photos (Fig. 8a) that numerous black circular pits on the uncoated Mg metal surface after carrying out the electrochemical corrosion test in the solution, while, there were few pits on the coated substrates. In addition, there were no significant differences in the corrosion potential and corrosion current density among the coatings. Moreover, the glass (sample MP0) and composite (sample MP10) coatings significantly ($p < 0.05$) decreased the corrosion potential of Mg metal substrates compared to the uncoated ones. While the effect of MP30 coating was insignificant ($p > 0.06$). Similarly, the corrosion current densities of the coated samples; MP0 and MP10 (0.0049 and 0.0048 $A.cm^{-2}$, respectively) were significantly ($p < 0.03$) less than that of uncoated sample (0.1443 $A.cm^{-2}$), whereas, the difference of the corrosion current density of Mg metal and MP30 (0.0051 $A.cm^{-2}$) was insignificant ($p > 0.077$). Accordingly, the inclusion of Mg-phosphate ceramic in the coating was useful to increase the corrosion resistance under 30 wt. %. As mentioned before, the coating containing 30 wt. % Mg-phosphate (sample MP30) was possessed the highest hydrophilicity, as well as, it characterized by crack

Table 2 The corrosion current density (i_{corr}), corrosion potential (E_{corr}), and corrosion resistance are obtained from polarization curves

	Current density i_{corr} (A/cm2)	Potential E_{corr} (V)	Corrosion rate P_i (mm/year)
Mg	0.144 ± 0.005	-1.481 ± 0.144	3.3
MP0	0.005 ± 0.003	-1.092 ± 0.039	0.11
MP10	0.005 ± 0.002	-1.097 ± 0.231	0.11
MP30	0.005 ± 0.004	-1.166 ± 0.237	0.12

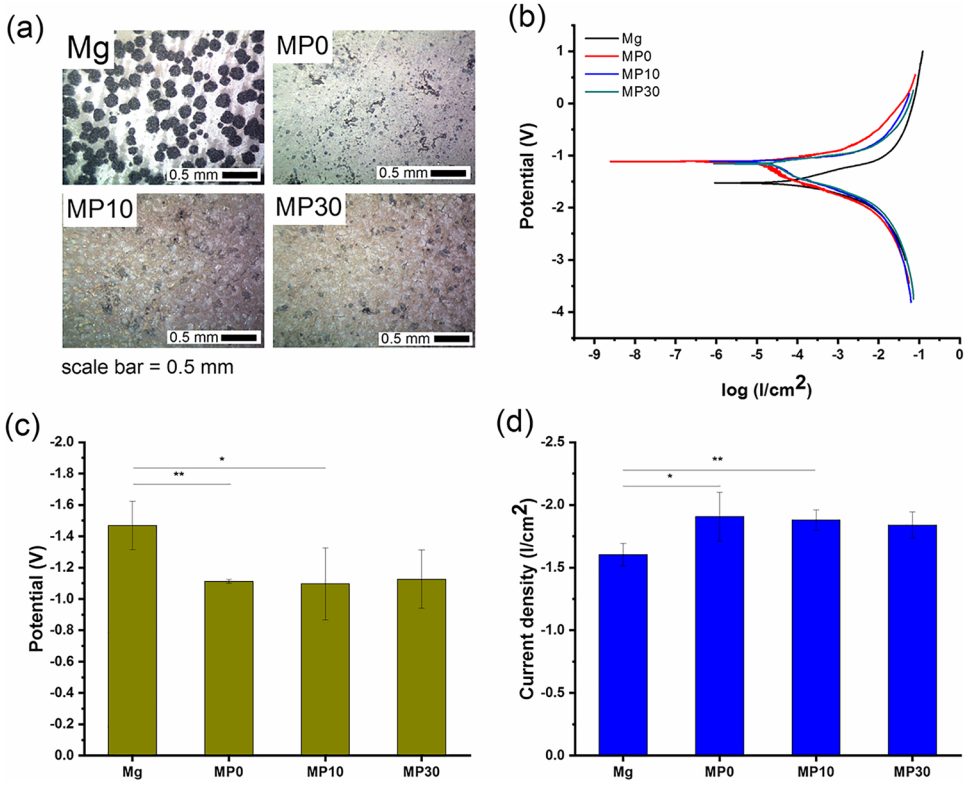

Fig. 8 (**a**) optical microscope photos, (**b**) potentiodynamic polarization curves, (**c**) potential, V, and (**d**) current density of Mg metal and coated substrates (MP0, MP10, and MP30) electrochemically tested in Hank's solution at 37 °C. *$p < 0.05$ and **$p < 0.02$

propagation and high surface roughness. These properties made the electrochemical corrosion process easier.

The corrosion current density was used to determine the average corrosion rate P_i (mm/year) which was calculated from The potentiodynamic polarization curves by extrapolation of the corrosion current density based on the following equation [48]:

$$Pi = 22.85\ i_{corr}$$

As stated before, the uncoated Mg metal had the largest i_{corr} (0.1443 A.cm^{-2}) and so the calculated corresponding corrosion rate was 3.3 mm/year (Table 2). The corrosion rates of the coated samples nearly were thirteen times lower than those of the uncoated Mg metal. The results indicated that the glass and composite coatings significantly improved the corrosion resistance of Mg alloy, implying that bioglass and bioglass/Mg-phosphate worked as a high-efficiency inhibitor for Mg corrosion in the medium. This mechanism is presented in Fig. 9. The few cracks propagated in the glass coating (sample MP0) and coating contained 10 wt. %

Table 3 CC_{50} values of Mg metal and coated substrates (MP0, MP10, and MP30)

Sample	CC50 (µg/ml)
Mg	368 ± 2.14
MP0	240 ± 1.58
MP10	293 ± 2.01
MP30	238 ± 1.16

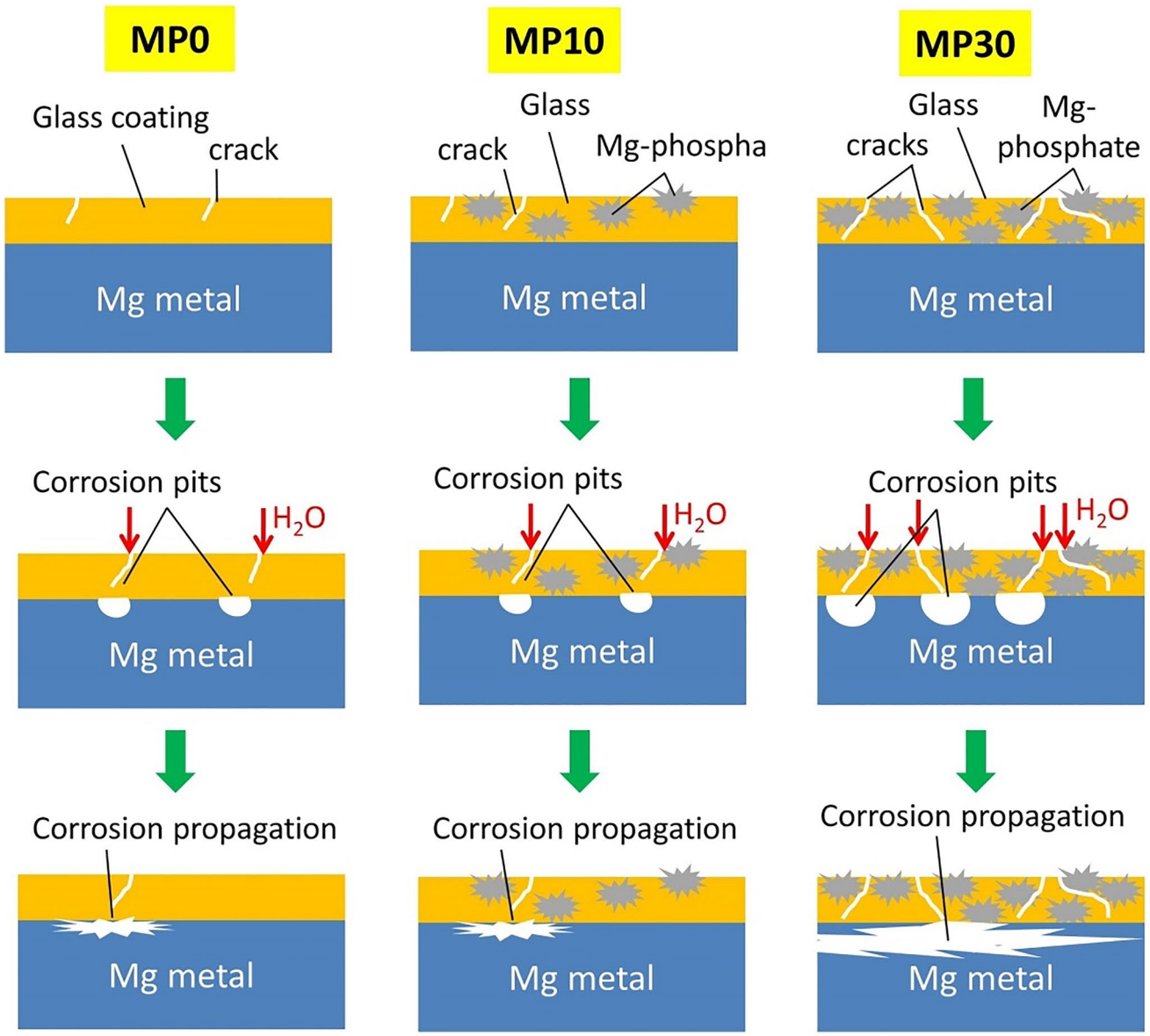

Fig. 9 Graphical presentation showing comparative corrosion mechanism of MP0, MP10, and MP30. In the case of MP30 sample, the crack propagation and high roughness resulted from large wt. % of Mg-phosphate caused more corrosion of Mg metal substrate

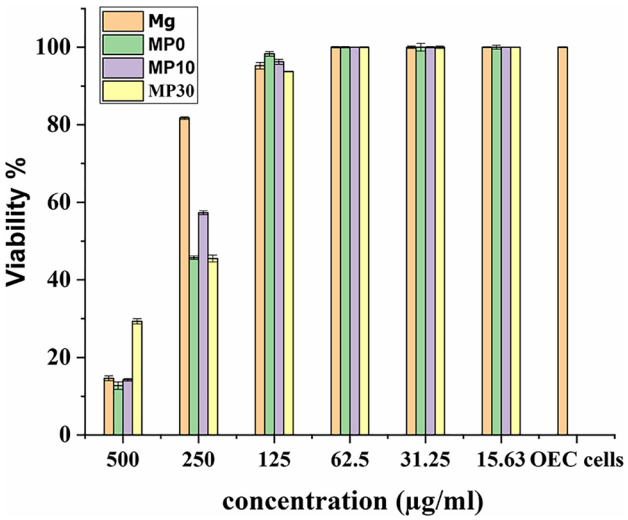

Fig. 10 Biocompatibility assay of Mg metal and coated substrates (MP0, MP10, and MP30) against oral epithelial cells (OEC) cell line

Mg-phosphate (sample MP10), while increase of amount of Mg-phosphate up to 30 wt. % generated more cracks in the coating. These cracks acted as channels to pass the water to the metal surface and starting corrosion pits of this surface. The pit area increased progressively with the time causing coating lose. This corrosion process was a little bit deeper for MP30 than MP0 and MP10 due to presence of larger numbers of crack throughout the coating of MP30 sample.

4.8 Biocompatibility assay

The CC50 values were used to calculate the viability of oral epithelial cells to magnesium metal, glass, and composites. The four treatments examined in this assay were Mg, MO, MP10, and MP30. Table 3 lists the CC50 values for each treatment. The findings demonstrated that Mg had the lowest level of cytotoxicity, followed by MP10, MP0, and MP30, with

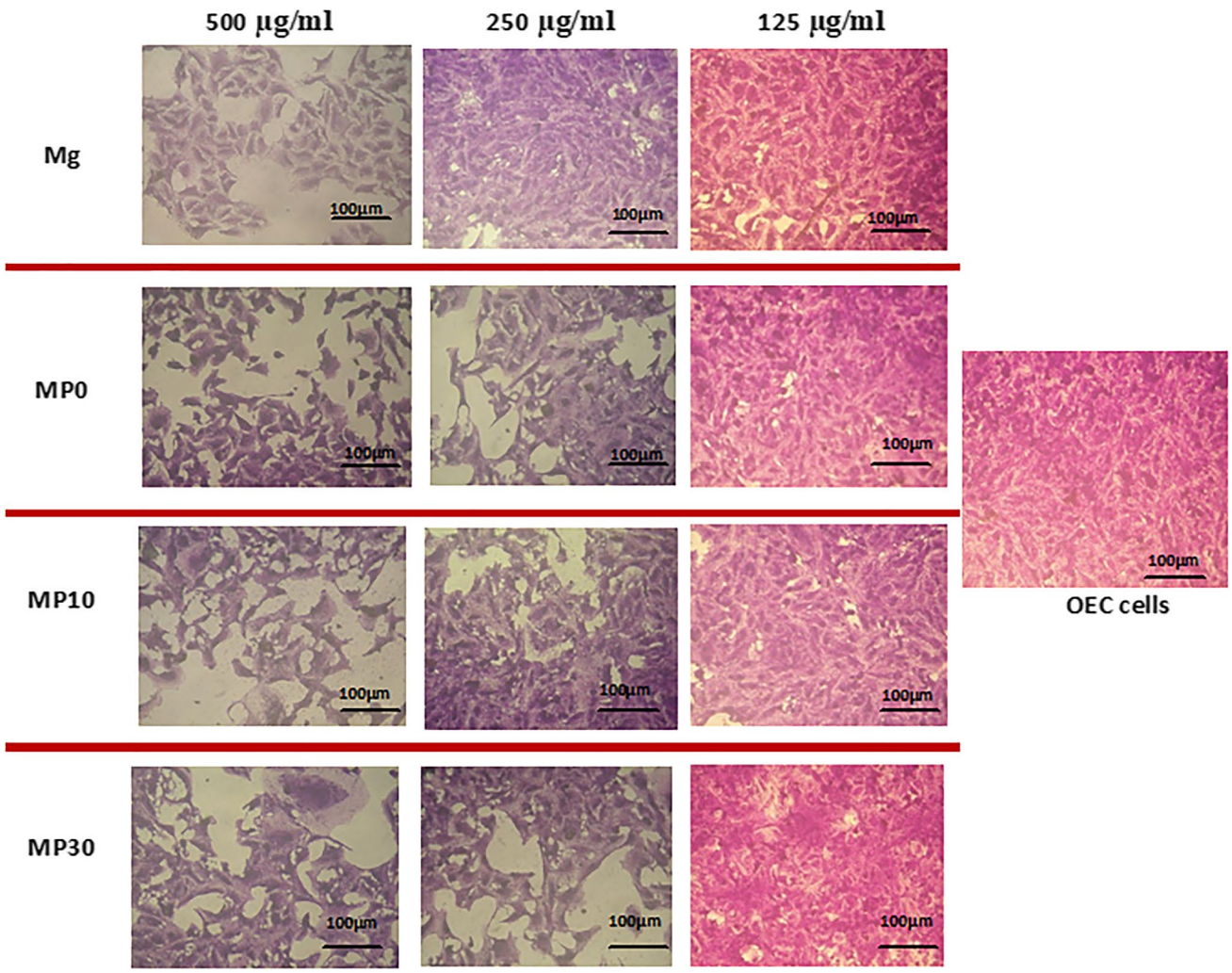

Fig. 11 Photos of oral epithelial cells after treatment by Mg metal and coated substrates (MP0, MP10, and MP30). Magnification: ×40

CC50 values of 368, 293, 240, and 238 g/ml, respectively. Higher inhibitory activity was detected for each sample at a higher concentration of 500 µg/ml. While at a concentration of 250 µg/ml, the viability percent was increased to 81.75, 57.33, 45.75, and 45.51 for Mg, M10, MP0, and MP30, respectively. No cytotoxic effect appeared at a lower concentration from 125 to15.36 µg/ml (Fig. 10). The previous results are supported by the results of the images captured by the inverted microscope (Fig. 11) at concentrations from 500 to 125 µg/ml, which confirmed the increase in the percentage of live cells with an increase in dilution for each treatment from 500 to 125 µg/ml.

The higher inhibitory activity of Mg, MP0, MP10, and MP30 at a higher concentration of 500 µg/ml remains in the Mg^{2+} and Ca^{2+} ions released from the magnesium metal and glass or composites, which increases the alkalinity of the surrounding media. Any defect in the pH leads to imbalance and causes cells to be affected. According to the bioactivity assay, the measurement of calcium ions in different solutions showed that the MP10 sample has a low concentration of calcium due to consuming calcium ions in forming a new apatite layer. Thus Mg and MP10 coating was more compatible with oral cells than the other coatings [24, 42].

5 Conclusion

Coating of Mg alloys with Mg-phosphate is usually performed by complex and costly methods, such as arc oxidation and plasma oxidation. Herein, we successfully applied a simple spin coating method for coating Mg metal with Mg-phosphate using the so-gel method. Where Mg-phosphate ceramic particles were dispersed in the glass sol ($85SiO_2$-$10CaO$-$5P_2O_5$ system) during the coating process. On the other hand, Mg-phosphate ceramic was used with different percentages (0, 10, and 30 wt. %) to tailor the physical and chemical properties of the coating. All coatings enhanced the formation of apatite-bone like layer on the Mg metal surface, and they were viable with oral epithelial cells at a concentration ≤ 125 µg/ml. Moreover, MP0 and MP10 coatings significantly enhanced the corrosion resistance of the metal, while, MP30 coating did not show a significant effect on it. Thus, the percentage of Mg-phosphate in the coating was beneficial for corrosion resistance when it was ≤ 10 wt. %. As a result, such composites showed promising coatings to decrease the corrosion of Mg metal implants by the inclusion of low percentages of Mg-phosphate ceramic.

Acknowledgements We would like to thank the National Research Centre, and Faculty of Science, Al-Azhar University (Girls), Egypt for the possibility to use their facilities.

Authors' Contributions Mohammad M. Farag: Conceptualization, Methodology, Writing Original draft preparation. Hanaa Y. Ahmed: Methodology, Data curation. Zainab M. Al-Rashidy: Methodology, Data curation, Writing Original draft preparation.

Funding Open access funding provided by The Science, Technology & Innovation Funding Authority (STDF) in cooperation with The Egyptian Knowledge Bank (EKB).

DAta Availability The data and materials that have been used in this work is not available to be shared, they are confidential data.

Declarations

Ethics Approval and Consent to Participate Not applicable.

Consent for Publication Not applicable.

Competing Interests The authors declare that they have no conflict of interest.

References

1. Tong P et al (2022) Recent progress on coatings of biomedical magnesium alloy. Smart Materials in Medicine 3:104–116
2. Staiger MP et al (2006) Magnesium and its alloys as orthopedic biomaterials: a review. Biomaterials 27(9):1728–1734
3. Kirkland NT (2012) Magnesium biomaterials: past, present and future. Corros Eng, Sci Technol 47(5):322–328
4. Virtanen S (2011) Biodegradable Mg and Mg alloys: Corrosion and biocompatibility. Mater Sci Eng, B 176(20):1600–1608
5. Agarwal S et al (2016) Biodegradable magnesium alloys for orthopaedic applications: A review on corrosion, biocompatibility and surface modifications. Mater Sci Eng, C 68:948–963
6. Song G (2005) Recent progress in corrosion and protection of magnesium alloys. Adv Eng Mater 7(7):563–586
7. Song G (2007) Control of biodegradation of biocompatable magnesium alloys. Corros Sci 49(4):1696–1701
8. Song G-L (2013) Corrosion prevention of magnesium alloys. Elsevier
9. Ding Y et al (2014) Effects of alloying elements on the corrosion behavior and biocompatibility of biodegradable magnesium alloys: a review. Journal of materials chemistry B 2(14):1912–1933
10. Samant AN, Dahotre NB (2009) Laser machining of structural ceramics—A review. J Eur Ceram Soc 29(6):969–993
11. Banerjee PC et al (2011) Electrochemical investigation of the influence of laser surface melting on the microstructure and corrosion behaviour of ZE41 magnesium alloy–An EIS based study. Corros Sci 53(4):1505–1514

12. Zou Y-H et al (2019) Corrosion resistance and antibacterial activity of zinc-loaded montmorillonite coatings on biodegradable magnesium alloy AZ31. Acta biomaterialia
13. Ashassi-Sorkhabi H et al (2019) Hybrid sol-gel coatings based on silanes-amino acids for corrosion protection of AZ91 magnesium alloy: Electrochemical and DFT insights. Prog Org Coat 131:191–202
14. Bosco R et al (2012) Surface engineering for bone implants: a trend from passive to active surfaces. Coatings 2(3):95–119
15. Mashtalyar DV et al (2022) Antibacterial Ca/P-coatings formed on Mg alloy using plasma electrolytic oxidation and antibiotic impregnation. Mater Lett 317:132099
16. Shi H et al (2021) Biodegradable polyacrylate copolymer coating for bio-functional magnesium alloy. Prog Org Coat 159:106422
17. Nadaraia KV et al (2021) Some new aspects of the study of dependence of properties of PEO coatings on the parameters of current in potentiodynamic mode. Surf Coat Technol 426:127744
18. Muresan L (2015) Intelligent Coatings for Corrosion Control. Elsevier Amsterdam
19. Hench LL et al (1971) Bonding mechanisms at the interface of ceramic prosthetic materials. J Biomed Mater Res 5(6):117–141
20. Hench LL (1998) Bioactive materials: the potential for tissue regeneration. J Biomed Mater Res 41(4):511–518
21. Rahaman MN et al (2011) Bioactive glass in tissue engineering. Acta Biomater 7(6):2355–2373
22. Vallet-Regí M, Ragel CV, Salinas AJ (2003) Glasses with medical applications. Eur J Inorg Chem 2003(6):1029–1042
23. Kaur M, Singh H, Prakash S (2008) A survey of the literature on the use of high velocity oxy-fuel spray technology for high temperature corrosion and erosion-corrosion resistant coatings. Anti-Corrosion Methods and Materials
24. Farag MM, Liu HH, Makhlouf AH (2021) New Nano-Bioactive Glass/Magnesium Phosphate Composites by Sol-Gel Route for Bone Defect Treatment. SILICON 13(3):857–865
25. Farag M, Yun H-S (2014) Effect of gelatin addition on fabrication of magnesium phosphate-based scaffolds prepared by additive manufacturing system. Mater Lett 132:111–115
26. Lee J et al (2014) A simultaneous process of 3D magnesium phosphate scaffold fabrication and bioactive substance loading for hard tissue regeneration. Mater Sci Eng, C 36:252–260
27. Farag MM et al (2020) The combined antibacterial and anticancer properties of nano Ce-containing Mg-phosphate ceramic. Life Sci 257:117999
28. Tamimi F et al (2011) Biocompatibility of magnesium phosphate minerals and their stability under physiological conditions. Acta Biomater 7(6):2678–2685
29. Moseke C, Saratsis V, Gbureck U (2011) Injectability and mechanical properties of magnesium phosphate cements. J Mater Sci - Mater Med 22(12):2591–2598
30. Wagh AS, Primus C (2006) Method and product for phosphosilicate slurry for use in dentistry and related bone cements. Google Patents
31. Van Phuong N, Moon S (2014) Comparative corrosion study of zinc phosphate and magnesium phosphate conversion coatings on AZ31 Mg alloy. Mater Lett 122:341–344
32. Ye X et al (2012) Bioactive glass–ceramic coating for enhancing the in vitro corrosion resistance of biodegradable Mg alloy. Appl Surf Sci 259:799–805
33. Bai K et al (2012) Fabrication of chitosan/magnesium phosphate composite coating and the in vitro degradation properties of coated magnesium alloy. Mater Lett 73:59–61
34. Anawati A, Hidayati E, Labibah H (2021) Characteristics of magnesium phosphate coatings formed on AZ31 Mg alloy by plasma electrolytic oxidation with improved current efficiency. Mater Sci Eng, B 272:115354
35. Oyane A et al (2003) Preparation and assessment of revised simulated body fluids. Journal of Biomedical Materials Research Part A: An Official Journal of The Society for Biomaterials, The Japanese Society for Biomaterials, and The Australian Society for Biomaterials and the Korean Society for Biomaterials 65(2):188-195
36. Jiang W et al (2018) In vitro evaluation of MgSr and MgCaSr alloys via direct culture with bone marrow derived mesenchymal stem cells. Acta Biomater 72:407–423
37. Johnson I et al (2016) A systemic study on key parameters affecting nanocomposite coatings on magnesium substrates. Acta Biomater 36:332–349
38. Park HY et al (2009) Characteristics of organic–inorganic hybrid coating films synthesized from colloidal silica-silane sol. J Electroceram 22(1–3):309–314
39. Mioč EK, Gretić ZH, Ćurković HO (2018) Modification of cupronickel alloy surface with octadecylphosphonic acid self–assembled films for improved corrosion resistance. Corros Sci 134:189–198
40. Menzies KL, Jones L (2010) The impact of contact angle on the biocompatibility of biomaterials. Optom Vis Sci 87(6):387–399
41. Goh Y-F et al (2014) In-vitro characterization of antibacterial bioactive glass containing ceria. Ceram Int 40(1):729–737
42. Kokubo T et al (1990) Ca, P-rich layer formed on high-strength bioactive glass-ceramic A-W. J Biomed Mater Res, Part A 24(3):331–343
43. Song G et al (1997) The anodic dissolution of magnesium in chloride and sulphate solutions. Corros Sci 39(10–11):1981–2004
44. Zhang Y et al (2005) Electrochemical behavior of anodized Mg alloy AZ91D in chloride containing aqueous solution. Corros Sci 47(11):2816–2831
45. Farag MM et al (2022) Comparative study of Mg-phosphate/cellulose and struvite/cellulose composites: Green synthesis, degradation, and biocompatibility. Bioactive Carbohydrates and Dietary Fibre, p. 100337
46. Farag MM et al (2022) Dental pulp stem cell viability and osteogenic potential assessment of new Mg-phosphate magnetic bioceramic nanoparticles. J Mater Res 37(2):595–607
47. Chiu K et al (2007) Characterization and corrosion studies of fluoride conversion coating on degradable Mg implants. Surf Coat Technol 202(3):590–598
48. Shi Z, Liu M, Atrens A (2010) Measurement of the corrosion rate of magnesium alloys using Tafel extrapolation. Corros Sci 52(2):579–588